Coherence gate manipulation for enhanced imaging through scattering media by non-ballistic light in partially coherent interferometric systems

ĎURIŠ, M.; CHMELÍK, R.

Optics Letters, vol. 46, iss. 18, pp. 4486-4489

ISSN: 0146-9592

DOI: https://doi.org/10.1364/OL.432484

Accepted manuscript

Coherence gate manipulation for enhanced imaging through scattering media by non-ballistic light in partially coherent interferometric systems

MIROSLAV ĎURIŠ[1,*] AND RADIM CHMELÍK[1,2]

[1] CEITEC – Central European Institute of Technology, Brno University of Technology, Purkyňova 656/123, 61200 Brno, Czech Republic
[2] Institute of Physical Engineering, Faculty of Mechanical Engineering, Brno University of Technology, Technická 2896/2, 61669 Brno, Czech Republic
[*] Corresponding author: miroslav.duris@ceitec.vutbr.cz

Compiled July 27, 2021

Coherence gating is typically exploited for imaging through disordered media by least-scattered (ballistic) light. Ballistic light based approaches produce clear images only when the proportion of ballistic to multiply scattered (non-ballistic) light is relatively high. To overcome this limitation, we counterintuitively utilize the coherence gate to image by the non-ballistic light, enabling us to retrieve information missing in the ballistic image. We show that non-ballistic images acquired by a transversal coherence gate shifting have image quality and spatial resolution comparable to the ballistic image. Combining images for different coherence gate positions, we synthesize an image of quality superior to ballistic light approaches. We experimentally demonstrate our concept on quantitative phase imaging through biological tissue.

http://dx.doi.org/10.1364/ao.XX.XXXXXX

One of the principal challenges in biomedical research is imaging through turbid media [1]. Optical imaging methods tackling this problem strive to minimize the effect of the random multiply scattered light [2] or to control it optically or digitally [3]. The first group methods increasingly utilize the so-called coherence-gating effect [4, 5]. This filtering phenomenon arises from a limited spatial and temporal coherence of illumination. Therefore, it is intrinsic to partially coherent optical systems. Imaging techniques that use the coherence gate for separating only the ballistic (scattered by the object only) light from the unwanted multiply scattered (non-ballistic) light include optical coherence tomography and microscopy [6], achromatic digital holography [7, 8], Horn microscopy [9] or white-light diffraction tomography [10]. In comparison to coherent one, the partially coherent illumination provides them numerous advantageous imaging properties such as higher spatial resolution, depth sectioning, and speckle noise reduction [8]. Despite these advantages, coherent beams are frequently used in optical systems because of their simple experimental implementation and well-defined parameters described by a complex two-dimensional function allowing straight-forward inverse modeling [11].

Partially coherent beams require for the complete description at least four-dimensional function making them less convenient for computational imaging [12]. The most common representations include cross-spectral density, mutual coherence function (MCF), and phase-space distributions [12]. Their experimentally challenging measurement is redeemed by being irreplaceable in illumination source characterization [13], crystal structure determination [14], three-dimensional object reconstruction [15], object tracking behind opaque structures [16] or quantification of light diffusion parameters of scattering specimen [17]. Heterodyne imaging [18] and spatial light modulator [19] have been employed to obtain phase-space distribution. Complete second-order correlation measurements have been demonstrated by coherence holography [20] or using a pinhole array mask [21]. As a consequence of permanently setting the coherence gate to a position separating only the ballistic light, the imaging techniques [6–10] are unable (in their standard arrangements) to measure complete MCF, and therefore, fully utilize their potential.

In this letter, we demonstrate the principal importance of the complete mutual coherence function measurement for partially coherent interferometric imaging of objects with strongly scattering surroundings. We show that MCF describing the cross-correlation between the object and reference beam comprises the image information formed by both the ballistic and non-ballistic light. In addition to the ballistic image, we extract from the complete MCF by coherence gate manipulation images formed by the non-ballistic light fractions. If the turbid medium is rather weakly scattering, the ballistic light contains almost unaltered specimen information. However, when the scattering is stronger and the ballistic to multiply scattered light ratio is poor, the complementary non-ballistic light components can significantly improve insufficient ballistic imaging. Combining all the scattered light components, we demonstrate high-quality quantitative phase imaging throughout the entire field of view (FOV), even in experimental situations with a completely corrupted ballistic image.

To demonstrate the ideas mentioned above, we begin with a

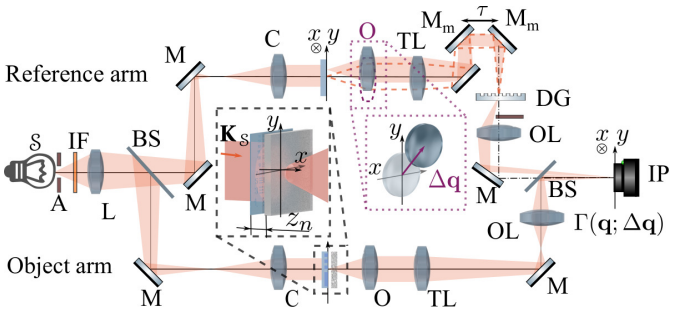

Fig. 1. Optical setup of the coherence-controlled holographic microscope: light source ($\mathcal{S}$), aperture (A), interference filter (IF), relay lens (L), beam splitters (BS), mirrors (M), movable mirrors (M_m), condensers (C), objective lenses (O), tube lenses (TL), diffraction grating (DG), output lenses (OL), interference plane (IP).

theoretical description of the MCF measurement in the optical setup used for the experimental part. We used a coherence-controlled holographic microscope (CCHM) [8], commercially available as Telight Q-Phase. The optical setup (see Fig. 1) consists of the object and reference arm, which contain optically equivalent microscope systems with a scattering object present in the object arm. The diffraction grating DG is implemented according to principles proposed by Leith [7] in the reference arm to ensure a formation of an off-axis hologram in the interference plane IP. The fundamental image properties depend on the parameters of condensers C and objective lenses O in couples with tube lenses TL characterized by the pupil functions (see Ref. 22) P_C and P_O, respectively. The axes x, y of the object space Cartesian coordinate system lie in the object plane, and the axis z points in the optical axis direction (see Fig. 1). The position of a point in the image plane is specified by the coordinates of the optically conjugated point $\mathbf{q} = (x, y)$ in the object plane. A halogen lamp $\mathcal{S}$ filtered by an interference filter IF (central wavelength 650 nm and 10 nm full width at half maximum) provides thermal, spatially broad, and quasi-monochromatic illumination. It is imaged to the object focal planes of the condensers forming Köhler illumination. The transverse wave vector coordinates $\mathbf{K}_\mathcal{S}$ of a plane wave behind condensers are proportional to the respective source point coordinates. For this reason, the source properties can be characterized by a function of $\mathbf{K}_\mathcal{S}$. We use reduced wave vector notation $|\mathbf{K}| = 1/\lambda$, where λ is the wavelength of light, and $\mathbf{K} = (\mathbf{K}_t, K_z) = (K_x, K_y, K_z)$, where $\mathbf{K}_t$ is the transverse wave vector and $K_z = \sqrt{|\mathbf{K}|^2 - |\mathbf{K}_t|^2}$.

From the time-averaged intensity measurements in IP, we digitally retrieve the cross-correlation information between object-scattered and reference light by a carrier removal in the Fourier plane [8]. The cross-correlation term dependent on the transversal displacement $\Delta\mathbf{q} = (\Delta x, \Delta y)$ and relative time-delay τ of the object-scattered and reference field can be understood as their mutual coherence function $\Gamma(\mathbf{q}, \mathbf{q} - \Delta\mathbf{q}, \tau)$. Therefore, interferometric imaging for a given time-delay τ and transverse displacement $\Delta\mathbf{q}$ is a partial MCF measurement. Modulus and phase image for particular $\Delta\mathbf{q}$ and τ is obtained as modulus and argument of Γ, respectively. The acquisition of MCF (complex-valued images) for all accessible $\Delta\mathbf{q}$ and τ makes the measurement complete. The complete MCF is available to every partially coherent interferometric system, where reference field position and optical path difference can be manipulated. In our system it is controlled by the reference arm elongation and objective shift (see Fig. 1). We further show that the most common arrangement of imaging setups fixed at $\tau = 0$ and $\Delta\mathbf{q} = (0, 0)$ corresponds to the ballistic light imaging while the MCF at $\Delta\mathbf{q} \neq (0, 0)$ carries significant amount of information about the non-ballistic imaging processes. As the coherence gating effect is mainly related to the low spatial coherence in transmitted-light systems, while temporal coherence has the influence of the second order [23], we discuss only manipulation with $\Delta\mathbf{q}$ in this letter. Given a complete spatial source incoherence, the expression for the measured MCF for $\tau = 0$ has according to Eq. (4.4-31) in Ref. 24 the form

$$\Gamma(\mathbf{q}, \mathbf{q} - \Delta\mathbf{q}) = \iint_{-\infty}^{\infty} |P_C(\mathbf{K}_\mathcal{S})|^2 \times h_o(\mathbf{K}_\mathcal{S}, \mathbf{q}) h_r^*(\mathbf{K}_\mathcal{S}, \mathbf{q} - \Delta\mathbf{q}) \mathrm{d}^2\mathbf{K}_\mathcal{S}, \quad (1)$$

where $h_o(\mathbf{K}_t, \mathbf{q})$ and $h_r(\mathbf{K}_t, \mathbf{q} - \Delta\mathbf{q})$ describe the propagation of a plane wave $\mathbf{K}_t$ through the object and reference arm, respectively.

The propagation of a plane wave through an object and imaging system is derived similarly to Ref. 22 assuming the multi-slice model of a volumetric specimen [25]. For simplicity, we neglect backscattering, and only small angles of propagation are assumed. The object is formed by a set of layers with spatial frequency spectra $T_n(\mathbf{Q}_n)$ in axial positions z_n of the object space, where $n \in N = \{A \ldots -2, -1, 0, 1, 2 \ldots B\}$. Negative n refers to $z_n < 0$, positive n refers to $z_n > 0$ and $n = 0$ denotes the in-focus layer. The propagation of a plane wave in the object path can be then described by

$$h_o(\mathbf{K}_t, \mathbf{q}) = \mathrm{e}^{2\pi\mathrm{i}\mathbf{q}\cdot\mathbf{K}_t} \int \ldots \int P_O\Big(\mathbf{K}_t + \sum_n \mathbf{Q}_n\Big) \times \prod_n T_n'(\mathbf{Q}_n) \mathrm{e}^{2\pi\mathrm{i}\mathbf{Q}_n\cdot[(\mathbf{K}_t + \sum_m \mathbf{Q}_m) z_n/K + \mathbf{q}]} \mathrm{d}^2\mathbf{Q}_n \quad (2)$$

where $T_n'(\mathbf{Q}_n) = T_n(\mathbf{Q}_n) \exp(\pi\mathrm{i} z_n |\mathbf{Q}_n|^2/K)$ and $\mathbf{Q}_n = (X_n, Y_n)$ is scattering vector in the n-th layer. The integrals go from $-\infty$ to ∞. The sum in the exponential indexed by $m \in N$ goes only through $m < n$. The reference field propagation can be described by $h_r(\mathbf{K}_t, \mathbf{q} - \Delta\mathbf{q}) = P_O(\mathbf{K}_t) \exp\{2\pi\mathrm{i}[\mathbf{K}_t \cdot (\mathbf{q} - \Delta\mathbf{q})]\}$. If we neglect diffraction by objective apertures setting $P_O = 1$, then it is evident how illumination source properties affect MCF measurement and give rise to the coherence-gating effect. Plugging Eq. (2) into Eq. (1) one obtains MCF in the following form

$$\Gamma(\mathbf{q}; \Delta\mathbf{q}) \approx \int \ldots \int t_0\Big(\mathbf{q} + \sum_{n \in N^+} \frac{z_n}{K} \mathbf{Q}_n\Big) \mathcal{G}\Big(\sum_{n \in N_0} \frac{z_n}{K} \mathbf{Q}_n + \Delta\mathbf{q}\Big) \times \prod_{n \in N_0} T_n'(\mathbf{Q}_n) \mathrm{e}^{2\pi\mathrm{i}\mathbf{Q}_n\cdot[\sum_m \mathbf{Q}_m z_n/K + \mathbf{q}]} \mathrm{d}^2\mathbf{Q}_n, \quad (3)$$

where $N^+ = \{1, 2, 3 \ldots B\}$ and $N_0 = N - \{0\}$. Function $\mathcal{G}(\Delta\mathbf{q}) = \iint_{-\infty}^{\infty} |P_C(\mathbf{K}_\mathcal{S})|^2 \exp[2\pi\mathrm{i}(\mathbf{K}_\mathcal{S} \cdot \Delta\mathbf{q})] \mathrm{d}^2\mathbf{K}_\mathcal{S}$ can be for a diffraction-limited condenser with the numerical aperture NA_C approximated using Bessel function of the first kind as $\mathcal{G}(\Delta\mathbf{q}) = 2J_1(\mu)/\mu$, where $\mu = 2\pi K \mathrm{NA}_C \Delta\mathbf{q}$. For example, using wavelength 650 nm and $\mathrm{NA}_C = 0.5$ the central Airy disk radius is 0.8 µm. Equation (3) shows that, in the case of imaging by multiply scattered light, MCF for each $\Delta\mathbf{q}$ can be understood as an image t_0 of the in-focus layer modulated by inverse Fourier transforms of expressions $T_n'(\mathbf{Q}_n) \exp(2\pi\mathrm{i}\mathbf{Q}_n \cdot \sum_m \mathbf{Q}_m z_n/K)$ filtered by a windowing function $\mathcal{G}$. The narrow central maximum of $\mathcal{G}$ ensures that only scattering event cascades satisfying

$\sum z_n \mathbf{Q}_n / K \approx -\Delta\mathbf{q}$ contribute to the image formation process, and also limits blurring of t_0 for $N_0 = N^+$. $T_n'(\mathbf{Q}_n)$ values dictate the degree of the contribution. Therefore, we call the function $\mathcal{G}$ a coherence-gating function (CGF).

Equation (3) also clarifies the CGF setting for the ballistic and non-ballistic imaging mode. Measuring MCF for CGF position $\Delta\mathbf{q} = (0,0)$ corresponds to $|\mathbf{Q}_n| = 0, \forall n \neq 0$, i.e., to the ballistic light imaging. It is evident that non-ballistic combinations of $\mathbf{Q}_n$ that satisfy $|\sum z_n \mathbf{Q}_n / K| \approx 0$ also affect the ballistic image. As mentioned earlier, these combinations are negligible only for weakly scattering surroundings. Therefore, in other cases, the image will not be perfect representation of the object in focus. The same also applies for MCF measurement for $\Delta\mathbf{q} \neq (0,0)$, the non-ballistic light imaging. Both ballistic and non-ballistic imaging obey the same equation, Eq. (3), and differ only by the parameter $\Delta\mathbf{q}$. Therefore, we further treat them equally.

It is instructive to demonstrate the principles first on a simplified case of imaging through a single scattering layer. We show that when the scattering by the surrounding medium is strong, non-ballistic light carries image information of the same quality as the ballistic light and that images formed are complementary. We demonstrate this claim on the case of quantitative phase imaging of a phase resolution target through an opaque etched glass plate separated by a coverslip, which defines the z_1 distance. For this experiment, we used 20x objectives with NA $= 0.5$ and illumination aperture was $\mathrm{NA_C} = 0.5$. The layer of interest was placed in the focus of the objective and imaged through the strongly scattering layer. We chose the scattering strength of the etched layer such that a bright-field image with partially coherent illumination, see Fig. 2(a), does not show any part of the resolution target. More importantly, not even coherence gated ballistic light provides high-enough quality throughout the whole field of view (FOV), see ballistic modulus and phase images in Fig. 2(c, d). We have measured the complete MCF with [purple curve in Fig. 2(b)] and without (orange curve) the scattering layer and we display the normalized modulus $|\gamma_\mathrm{R}| = |\Gamma_\mathrm{R}|/|\Gamma_{max}|$ for a point R [see Fig. 2(c)] against Δx in Fig. 2(b). Here $|\Gamma_{max}|$ stands for the highest possible value of $|\Gamma|$ in CCHM. In general, as the modulus drops, the quality of the image derived at that point of MCF degrades. There are two reasons, MCF modulus is in relationship to the root mean square error of phase measurement through inverse proportion (see Chap. 9.4.4 in Ref. 26), and phase singularities occupy near-zero modulus areas [27]. Therefore, the MCF modulus serves as an indicator of phase quality. Regarding the curves in Fig. 2(b) one can expect to acquire some information only in Δx points with a high modulus. It is evident that when imaging only a single planar object, the complete MCF measurement (orange curve) does not add any information to the ballistic mode. However, when we image through at least one additional strongly scattering layer, non-ballistic parts of MCF contain valuable information. The following adaptation of Eq. (3) for this simple case allows us to discuss the image properties for particular $\Delta\mathbf{q}$

$$\Gamma(\mathbf{q};\Delta\mathbf{q}) \approx \iint t_0\left(\mathbf{q} + \frac{z_1}{K}\mathbf{Q}_1\right)\mathcal{G}\left(\frac{z_1}{K}\mathbf{Q}_1 + \Delta\mathbf{q}\right) \times T_1'(\mathbf{Q}_1)\mathrm{e}^{2\pi\mathrm{i}\mathbf{Q}_1\cdot\mathbf{q}}\mathrm{d}^2\mathbf{Q}_1. \quad (4)$$

This equation suggests that each part of the MCF acquired for different $\Delta\mathbf{q}$ can be interpreted as an image t_0 of the resolution target shifted by $\Delta\mathbf{q}$. The scattering on the etched layer manifests itself as modulation by the inverse Fourier transform of the spatial frequency spectrum $T_1'(\mathbf{Q}_1)$. CGF limits this spectrum only to scattering vectors satisfying relation $\mathbf{Q}_1 z_1 / K \approx -\Delta\mathbf{q}$. The produced modulation appears to be random with high and low modulus areas. The stronger coherence-gating effect reduces more the range of contributing $T_1'(\mathbf{Q}_1)$ spatial frequencies, and therefore, the size of the high-modulus areas increases. This reduces the number of phase singularities and makes the additive phase from out-of-focus scattering more uniform. As the CGF allows a finite range of scattering layer components to contribute, the image is blurred. The blur is limited by CGF Airy disk radius, which defines the transversal spatial resolution. The real CGF width can be determined from the measurement without scattering layer in Fig. 2(b). For this experiment, it is 0.8 µm. We can conclude that the change of the imaging mode to non-ballistic light generally does not affect the size of high-quality phase areas or the resolving power. Therefore, neither of the imaging modes is inferior.

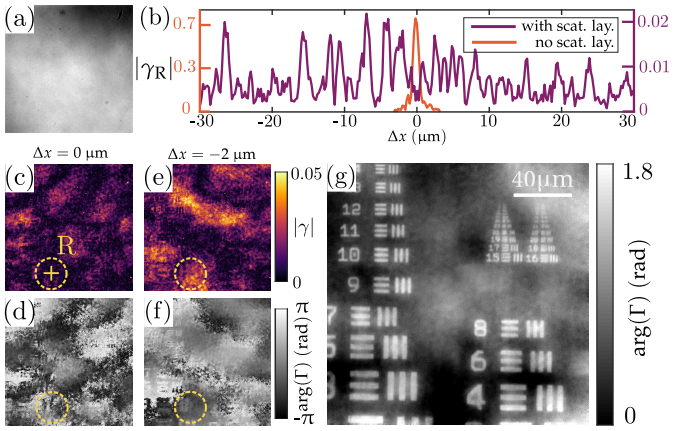

Fig. 2. Results for imaging of the phase resolution target through etched glass plate. (a) Bright-field ballistic imaging mode. (b) Normalized modulus of measured MCF against Δx at point R. Modulus (c), (e) and phase (d), (f) images derived from MCF for $\Delta\mathbf{q} = (0,0)$ µm (ballistic light image) and $\Delta\mathbf{q} = (-2,0)$ µm for imaging through the etched glass plate. (g) Synthetic quantitative phase image created by a combination of non-ballistic images. Objectives used $20\mathrm{x}/\mathrm{NA} = 0.5$, $\mathrm{NA_C} = 0.5$.

We also use this experiment to demonstrate the complementary nature of non-ballistic images. Consider, for example, a small region of FOV marked by the yellow dashed ring in Fig. 2(c-f). One can see that information about the object is missing in the ballistic light [see the zero modulus in Fig. 2(c) and the random phase in Fig. 2(d)]. The shape of the complete MCF in Fig. 2(b) indicates that the information might be present for particular $\Delta\mathbf{q} \neq (0,0)$ with a higher modulus. We show the image acquired for $\Delta\mathbf{q} = (-2,0)$ µm, see Fig. 2(e, f), to support this statement. The modulus is higher in the circled area, and the phase information is present. These findings suggest that a combination of images acquired for different $\Delta\mathbf{q}$ can provide information about the whole FOV.

We designed a method to reconstruct a high-quality synthetic image throughout the whole FOV from the measured MCF. We acquired images for an 11×11 grid of $\Delta\mathbf{q}$ centered at the ballistic position with the sampling 1 µm, based on the Airy disk radius of CGF to avoid overlap. We adapted an algorithm derived in our preliminary work for phase compensation [28]. First, we shift images to their correct positions based on the CGF position $\Delta\mathbf{q}$. Then, corresponding small regions of all 121 images are phase-corrected for linear phase distortions with the objective

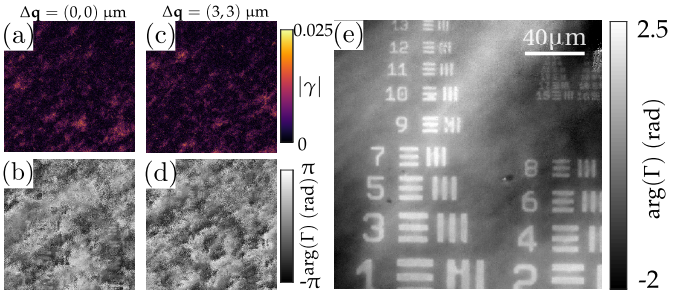

Fig. 3. Results for imaging through a slab of chicken breast. Modulus (a), (c) and phase (b), (d) images derived from MCF for $\Delta\mathbf{q} = (0,0)$ μm and $\Delta\mathbf{q} = (3,3)$ μm. (e) Synthetic quantitative phase image created by a combination of non-ballistic images. Objectives used $20\text{x}/\text{NA} = 0.5$, $\text{NA}_\text{C} = 0.3$.

to maximize the modulus of their coherent superposition. The phase quality is then after superposition significantly improved. A full FOV image is stitched together from smaller overlapping areas producing a high-quality quantitative phase image, and the result is displayed in Fig. 2(g). The phase quality is consistent throughout FOV and significantly improved in comparison to the ballistic light phase image in Fig. 2(d). The spatial resolution is also in agreement with the prediction. The smallest resolvable elements of the resolution target in Fig. 2(g) are 0.81 μm wide, which corresponds to the CGF width. It is important to note that coherent averaging of 121 ballistic images in this static case reduces low-contrast hologram noise but does not deal with the phase jumps and singularities, which are the main cause of image degradation. When the scattering medium is highly dynamic, averaging a high ballistic image number can provide similar image improvement as in Fig. 2(g) [29].

To verify the feasibility of our approach for imaging through turbid biological media, we carried out an experiment with a slab of chicken breast instead of the etched glass layer. The chicken breast was cut into a slab of thickness from 1 to 2 mm and squeezed between two coverslips separated by 0.8 mm thick ring. The chicken muscle tissue has transport mean free path of 1.25 mm, mean free path of 43.7 μm and an anisotropy factor of 0.965 [30]. One can see that neither ballistic [Fig. 3(a, b)] nor non-ballistic [Fig. 3(c, d)] images sufficiently reproduce the phase resolution target. We employed the same procedure as for the imaging through the etched glass plate. Even in this case it was possible to reconstruct a full FOV synthetic image [Fig. 3(e)] that carries qualitative and quantitative information of high quality. The spatial resolution is again in agreement with the theory.

In this letter, we first demonstrated theoretically and experimentally the equivalence between the complete MCF measurement and coherence-gated imaging for all accessible coherence gate positions in partially coherent interferometric systems. In the case of imaging through strongly scattering media, we showed that the coherence gate manipulation enables imaging by fractions of non-ballistic (multiply scattered) light, and that it carries complementary information to the ballistic image. Finally, we proved the immense value of using coherence-gated non-ballistic light by proposing a method for significant improvement of quantitative phase imaging quality through strongly scattering media. We carried out the experimental part using CCHM. However, a wide range of partially coherent interferometric systems can benefit from our outcomes. For example, the above mentioned imaging techniques [6–10] use the coherence gate to separate the ballistic light only. Nevertheless, they would be capable of measuring the complete MCF with slightly altered optical setups. Our approach then extends their imaging capabilities readily applicable in biomedical research.

Funding. This work was supported by the Grant Agency of the Czech Republic (No. 21-01953S), the MEYS CR (Large RI Project LM2018129 Czech-BioImaging) and the Specific Research grant of Brno University of Technology (No. FSI-S-20-6353).

Acknowledgments. M. Ď. is grateful for the support provided by the grant CEITEC VUT-J-20-6537 from BUT and Brno Ph.D. talent.

Disclosures. R. C.: Telight (P,R)

Data availability. Data underlying the results presented in this paper are not publicly available at this time but may be obtained from the authors upon reasonable request.

REFERENCES

1. S. Yoon, M. Kim, M. Jang, Y. Choi, W. Choi, S. Kang, and W. Choi, Nat. Rev. Phys. **2**, 141 (2020).
2. S. Kang, S. Jeong, W. Choi, H. Ko, T. D. Yang, J. H. Joo, J.-S. Lee, Y.-S. Lim, Q.-H. Park, and W. Choi, Nat. Photonics **9**, 253 (2015).
3. I. M. Vellekoop and A. P. Mosk, Opt. Lett. **32**, 2309 (2007).
4. M. R. N. Avanaki and A. Podoleanu, J. Biomed. Opt. **22**, 1 (2017).
5. O. Salhov, G. Weinberg, and O. Katz, Opt. Lett. **43**, 5528 (2018).
6. J. A. Izatt, E. A. Swanson, J. G. Fujimoto, M. R. Hee, and G. M. Owen, Opt. Lett. **19**, 590 (1994).
7. E. N. Leith and J. Upatnieks, J. Opt. Soc. Am. **57**, 975 (1967).
8. T. Slabý, P. Kolman, Z. Dostál, M. Antoš, M. Lošťák, and R. Chmelík, Opt. Express **21**, 14747 (2013).
9. D. Zicha and G. A. Dunn, J. Microsc. **179**, 11 (1995).
10. T. Kim, R. Zhou, M. Mir, S. D. Babacan, P. S. Carney, L. L. Goddard, and G. Popescu, Nat. Photonics **8**, 256 (2014).
11. Y. Cotte, F. Toy, P. Jourdain, N. Pavillon, D. Boss, P. Magistretti, P. Marquet, and C. Depeursinge, Nat. Photonics **7**, 113 (2013).
12. S. B. Mehta and C. J. R. Sheppard, J. Opt. Soc. Am. A **35**, 1272 (2018).
13. Y. Shao, X. Lu, S. Konijnenberg, C. Zhao, Y. Cai, and H. P. Urbach, Opt. Express **26**, 4479 (2018).
14. E. Wolf, Phys. Rev. Lett. **103**, 075501 (2009).
15. D. L. Marks, R. A. Stack, D. J. Brady, D. C. Munson, and R. B. Brady, Science **284**, 2164 (1999).
16. J. A. Newman, Q. Luo, and K. J. Webb, Phys. Rev. Lett. **116**, 073902 (2016).
17. A. Badon, D. Li, G. Lerosey, A. Claude Boccara, M. Fink, and A. Aubry, Optica **3**, 1160 (2016).
18. A. Wax and J. E. Thomas, Opt. Lett. **21**, 1427 (1996).
19. L. Waller, G. Situ, and J. W. Fleischer, Nat. Photonics **6**, 474 (2012).
20. D. N. Naik, T. Ezawa, R. K. Singh, Y. Miyamoto, and M. Takeda, Opt. Express **20**, 19658 (2012).
21. X. Lu, Y. Shao, C. Zhao, S. Konijnenberg, X. Zhu, Y. Tang, Y. Cai, and H. P. Urbach, Adv. Photonics **1**, 1 (2019).
22. R. Chmelik, M. Slaba, V. Kollarova, T. Slaby, M. Lostak, J. Collakova, and Z. Dostal, Prog. Opt. **59**, 267 (2014).
23. E. N. Leith, W.-C. Chien, K. D. Mills, B. D. Athey, and D. S. Dilworth, J. Opt. Soc. Am. A **20**, 380 (2003).
24. L. Mandel and E. Wolf, *Optical Coherence and Quantum Optics* (Cambridge University Press, 1995).
25. U. S. Kamilov, I. N. Papadopoulos, M. H. Shoreh, A. Goy, C. Vonesch, M. Unser, and D. Psaltis, Optica **2**, 517 (2015).
26. J. W. Goodman, *Statistical Optics* (Wiley, 2015), second edition ed.
27. N. Shvartsman and I. Freund, Opt. Commun. **117**, 228 (1995).
28. R. Chmelík, M. Duris, and L. Štrbková, "Quantitative phase imaging in turbid media by coherence controlled holographic microscopy," in *Unconventional Optical Imaging*, , vol. 10677 C. Fournier, M. P. Georges, and G. Popescu, eds., International Society for Optics and Photonics (SPIE, 2018), pp. 263 – 273.
29. A. V. Kanaev, A. T. Watnik, D. F. Gardner, C. Metzler, K. P. Judd, P. Lebow, K. M. Novak, and J. R. Lindle, Opt. Lett. **43**, 3088 (2018).
30. W. F. Cheong, S. A. Prahl, and A. J. Welch, IEEE J. Quantum Electron. **26**, 2166 (1990).

FULL REFERENCES

1. S. Yoon, M. Kim, M. Jang, Y. Choi, W. Choi, S. Kang, and W. Choi, "Deep optical imaging within complex scattering media," Nat. Rev. Phys. **2**, 141–158 (2020).
2. S. Kang, S. Jeong, W. Choi, H. Ko, T. D. Yang, J. H. Joo, J.-S. Lee, Y.-S. Lim, Q.-H. Park, and W. Choi, "Imaging deep within a scattering medium using collective accumulation of single-scattered waves," Nat. Photonics **9**, 253–258 (2015).
3. I. M. Vellekoop and A. P. Mosk, "Focusing coherent light through opaque strongly scattering media," Opt. Lett. **32**, 2309–2311 (2007).
4. M. R. N. Avanaki and A. Podoleanu, "En-face time-domain optical coherence tomography with dynamic focus for high-resolution imaging ," J. Biomed. Opt. **22**, 1 – 10 (2017).
5. O. Salhov, G. Weinberg, and O. Katz, "Depth-resolved speckle-correlations imaging through scattering layers via coherence gating," Opt. Lett. **43**, 5528 (2018).
6. J. A. Izatt, E. A. Swanson, J. G. Fujimoto, M. R. Hee, and G. M. Owen, "Optical coherence microscopy in scattering media," Opt. Lett. **19**, 590 (1994).
7. E. N. Leith and J. Upatnieks, "Holography with Achromatic-Fringe Systems*," J. Opt. Soc. Am. **57**, 975 (1967).
8. T. Slabý, P. Kolman, Z. Dostál, M. Antoš, M. Lošťák, and R. Chmelík, "Off-axis setup taking full advantage of incoherent illumination in coherence-controlled holographic microscope." Opt. Express **21**, 14747–62 (2013).
9. D. Zicha and G. A. Dunn, "An image processing system for cell behaviour studies in subconfluent cultures," J. Microsc. **179**, 11–21 (1995).
10. T. Kim, R. Zhou, M. Mir, S. D. Babacan, P. S. Carney, L. L. Goddard, and G. Popescu, "White-light diffraction tomography of unlabelled live cells," Nat. Photonics **8**, 256–263 (2014).
11. Y. Cotte, F. Toy, P. Jourdain, N. Pavillon, D. Boss, P. Magistretti, P. Marquet, and C. Depeursinge, "Marker-free phase nanoscopy," Nat. Photonics **7**, 113–117 (2013).
12. S. B. Mehta and C. J. R. Sheppard, "Partially coherent microscope in phase space," J. Opt. Soc. Am. A **35**, 1272 (2018).
13. Y. Shao, X. Lu, S. Konijnenberg, C. Zhao, Y. Cai, and H. P. Urbach, "Spatial coherence measurement and partially coherent diffractive imaging using self-referencing holography," Opt. Express **26**, 4479 (2018).
14. E. Wolf, "Solution of the phase problem in the theory of structure determination of crystals from X-ray diffraction experiments," Phys. Rev. Lett. **103**, 075501 (2009).
15. D. L. Marks, R. A. Stack, D. J. Brady, D. C. Munson, and R. B. Brady, "Visible Cone-Beam Tomography With a Lensless Interferometric Camera," Science **284**, 2164–2166 (1999).
16. J. A. Newman, Q. Luo, and K. J. Webb, "Imaging Hidden Objects with Spatial Speckle Intensity Correlations over Object Position," Phys. Rev. Lett. **116**, 073902 (2016).
17. A. Badon, D. Li, G. Lerosey, A. Claude Boccara, M. Fink, and A. Aubry, "Spatio-temporal imaging of light transport in highly scattering media under white light illumination," Optica **3**, 1160 (2016).
18. A. Wax and J. E. Thomas, "Optical heterodyne imaging and Wigner phase space distributions," Opt. Lett. **21**, 1427 (1996).
19. L. Waller, G. Situ, and J. W. Fleischer, "Phase-space measurement and coherence synthesis of optical beams," Nat. Photonics **6**, 474–479 (2012).
20. D. N. Naik, T. Ezawa, R. K. Singh, Y. Miyamoto, and M. Takeda, "Coherence holography by achromatic 3-D field correlation of generic thermal light with an imaging Sagnac shearing interferometer," Opt. Express **20**, 19658 (2012).
21. X. Lu, Y. Shao, C. Zhao, S. Konijnenberg, X. Zhu, Y. Tang, Y. Cai, and H. P. Urbach, "Noniterative spatially partially coherent diffractive imaging using pinhole array mask," Adv. Photonics **1**, 1 – 8 (2019).
22. R. Chmelik, M. Slaba, V. Kollarova, T. Slaby, M. Lostak, J. Collakova, and Z. Dostal, "The Role of Coherence in Image Formation in Holographic Microscopy," Prog. Opt. **59**, 267–335 (2014).
23. E. N. Leith, W.-C. Chien, K. D. Mills, B. D. Athey, and D. S. Dilworth, "Optical sectioning by holographic coherence imaging: a generalized analysis," J. Opt. Soc. Am. A **20**, 380–387 (2003).
24. L. Mandel and E. Wolf, *Optical Coherence and Quantum Optics* (Cambridge University Press, 1995).
25. U. S. Kamilov, I. N. Papadopoulos, M. H. Shoreh, A. Goy, C. Vonesch, M. Unser, and D. Psaltis, "Learning approach to optical tomography," Optica **2**, 517 (2015).
26. J. W. Goodman, *Statistical Optics* (Wiley, 2015), second edition ed.
27. N. Shvartsman and I. Freund, "Speckle spots ride phase saddles sidesaddle," Opt. Commun. **117**, 228–234 (1995).
28. R. Chmelík, M. Duris, and L. Štrbková, "Quantitative phase imaging in turbid media by coherence controlled holographic microscopy," in *Unconventional Optical Imaging,* vol. 10677 C. Fournier, M. P. Georges, and G. Popescu, eds., International Society for Optics and Photonics (SPIE, 2018), pp. 263 – 273.
29. A. V. Kanaev, A. T. Watnik, D. F. Gardner, C. Metzler, K. P. Judd, P. Lebow, K. M. Novak, and J. R. Lindle, "Imaging through extreme scattering in extended dynamic media," Opt. Lett. **43**, 3088–3091 (2018).
30. W. F. Cheong, S. A. Prahl, and A. J. Welch, "A Review of the Optical Properties of Biological Tissues," IEEE J. Quantum Electron. **26**, 2166–2185 (1990).